A gentle palette of plasma membrane dyes

Jing Ling[1,2,#], Yitong Liu [1,2,#], Yunzhe Fu[3], Shuzhang Liu[4], Ling Ding[5], Lulu Huang[6], Peng Xi[3], Zhixing Chen[1,2,7,8,*]

1. Peking-Tsinghua Center for Life Science, Academy for Advanced Interdisciplinary Studies, Peking University, Beijing 100871, China
2. College of Future Technology, Institute of Molecular Medicine, National Biomedical Imaging Center, Beijing Key Laboratory of Cardiometabolic Molecular Medicine, Peking University, Beijing 100871, China
3. Department of Biomedical Engineering, College of Future Technology, Peking University, Beijing 100871, China
4. College of Chemistry and Molecular Engineering, Synthetic and Functional Biomolecules Center Beijing National Laboratory for Molecular Sciences, Key Laboratory of Bioorganic Chemistry and Molecular Engineering of Ministry of Education, PKU-IDG/McGovern Institute for Brain Research, Peking University, Beijing, 100871, China
5. Center for Reproductive Medicine, Department of Obstetrics and Gynecology, Peking University Third Hospital, Beijing 100191 China
6. Peking University-Tsinghua University-National Institute of Biological Sciences Joint Graduate Program, Academy for Advanced Interdisciplinary Studies, Peking University, Beijing, China
7. PKU-Nanjing Institute of Translational Medicine, Nanjing 211800, China
8. Genvivo Biotech, Nanjing 211800, China

[#] These authors contributed equally to this work.

[*] E-mail: zhixingchen@pku.edu.cn (Z.C.)

Abstract

Plasma membrane stains are one of the most important organelle markers for unambiguous assignments of individual cells and monitoring membrane morphology and dynamics. The state-of-the-art PM stains are bright, specific, fluorogenic, and compatible with super-resolution imaging. However, when recording membrane dynamics, particularly under light-intensive microscopes, PM is prone to photodynamic damages due to its phospholipid bilayer nature. Here we developed PK Mem dyes tailored for time-lapse fluorescence imaging. By integrating triplet-state quenchers into the MemBright dyes featuring cyanine chromophores and amphiphilic zwitterion anchors, PK Mem dyes exhibited a three-fold reduction in phototoxicity and a more than four-fold improvement in photostability in imaging experiments. These dyes enable 2D and 3D imaging of live or fixed cancer cell lines and a wide range of primary cells, at the same time pair well with various fluorescent markers. PK Mem dyes can be applied to neuronal imaging in brain slices and *in vivo* two-photon imaging. The gentle nature of PK Mem palette enables ultralong-term recording of cell migration and cardiomyocyte beating. Notably, PK Mem dyes are optically compatible with STED/SIM imaging, which can handily upgrade the routine of time-lapse neuronal imaging, such as growth cone tracking and mitochondrial transportations, into nanoscopic resolutions.

Introduction

The plasma membrane (PM) is a dynamic structure separating the cell from the extracellular environment[1] and orchestrating substance transport[2], signal transduction[3, 4] and cell recognition[5]. Fluorescence imaging is one of the primary ways to study PM, such as in cell division, visualization of cell morphology, tracking membrane dynamics as well as monitoring intracellular and extracellular vesicles[6]. Therefore, strategies for fluorescently highlighting plasma membranes are instrumental in the visualization of membrane dynamics.

While it is possible to target genetically encoded fluorescent proteins to PM as imaging tags, chemical dyes offer more convenient and brighter staining of the PM, leading to their wider range of applications[6-8]. Achieving high specificity is the main quest of cell membrane imaging, and various strategies have been developed toward this goal. Exploiting antigen-antibody interaction between probes and surface antigen is an effective approach, giving a family of widely-used PM stains based on wheat germ agglutinin (WGA)-dye conjugate[9, 10]. However, due to the high molecular weight, WGA-iFluor™ 488 exhibits significant variability in intercellular staining and is prone to cellular endocytosis and dye internalization[11, 12]. In addition, it's reported that WGA-iFluor™ 488 can partially hinder the dynamics of the cell membrane[11]. Alternatively, chemical probes, bearing lower molecular weight and minimal perturbations to membranes, are developed and widely applied. These PM dyes are devised with membrane anchors and fluorophores, giving high labeling contrast through noncovalent interactions with phospholipids[13-18]. Generations of PM dyes, such as DiD, FM4-64, and Cell Mask, have been developed for cell membrane imaging[19-21]. However, each of them has certain inherent limitations. DiD and Cell Mask family dyes rely on hydrophobic interaction between long alkyl chains and cell membrane, resulting in probe internalization, high staining concentration and low solubility in working solution[18]. FM4-64 tends to translocate to the nuclear membrane at physiological temperatures due to its affinity for negatively charged lipids[22, 23]. Therefore, several strategies have been developed to address these issues. Among the emerging methods, the Klymchenko group reported the conjugation of amphiphilic zwitterionic anchors with various fluorophores, such as Nile Red[24, 25], squaraine[26], cyanine[12], and BODIPY[27] to create PM dyes capable of selectively and persistently staining cell membranes. One notable combination among them are MemBright dyes[12] (commercial name: MemGlow), consisting of cyanine and two amphiphilic zwitterionic anchors, which have found widespread applications with confocal microscopy, two-photon microscopy, and stochastic optical reconstruction microscopy.

On the flip side of the constantly evolving PM labeling strategies is the photophysical chemistry of the core fluorophores. In the past decade, the field has witnessed the transition from widefield and confocal imaging towards super-resolution and time-lapse imaging, which can monitor cell membrane morphology and dynamics at unprecedented spatial and temporal resolutions. However, the strong excitation schemes during imaging give rise to phototoxicity and photobleaching, leading to cell death and fluorescent signal disappearance during live imaging[28-30]. The reactive oxygen species (ROS) stemmed from the photosensitized dyes and molecular oxygen is believed to account for phototoxicity and photobleaching[31-34]. The PM, bearing unsaturated lipid with vulnerable olefin groups, exhibits greater sensitivity to ROS compared to other subcellular structures such as cytoskeleton, nucleus, or lipid droplet[35, 36]. Imaging-induced phototoxicity can impair the structure and function of the cell membrane,

88   leading to membrane blebbing, membrane rupture, and eventual cell death[37]. Consequently,
89   gentle fluorophores with low photodamage are becoming instrumental for future live-cell
90   recordings. Among the few chemical strategies that can alleviate phototoxicity and
91   photobleaching[38-41], intramolecular triplet-state quenching has stood out as one of the most
92   promising strategies. Originally proposed and demonstrated with cyclooctatetraene (COT)-
93   conjugated cyanine dyes and single-molecule applications[33, 39], TSQ-dye molecules have been
94   recently employed for live cell imaging applications including mitochondrial cristae imaging[34,
95   42], voltage imaging[43, 44], and chemigenetic protein imaging[33, 45]. COT-conjugation has generally
96   alleviated phototoxicity during time-lapse imaging at these selected cellular targets.

97   Herein, we reported PK Mem dyes, a palette of gentle PM dyes (Fig. 1A). Cyanine
98   chromophore, triplet state quenchers, and membrane anchors are elaborately integrated to PK
99   Mem molecules, giving excellent labeling efficiency of PM, reduced phototoxicity, and
100 enhanced photostability. PK Mem dyes can effectively stain cancer cell lines, primary cells, and
101 brain slices with high contrast. We demonstrate advanced applications including *in vivo* two-
102 photon imaging in a mouse brain, stimulated emission depletion (STED) imaging of dendritic
103 spines, time-lapse tracking of migrasomes, and SIM recording of mitochondrial movement in
104 axons. Practically, the phototoxicity of PK Mem dyes is less than one-third that of other
105 cyanine-based PM stains, offering the monitoring of cellular processes over remarkably
106 extended durations.

107

108 **Results**

109 *Design, synthesis, and characterizations of PK Mem dyes*

110 The design of gentle PM dyes with good specificity and low phototoxicity hinges on the
111 streamlined assembly of triplet-state quenchers and membrane anchors onto selected
112 fluorophores with practical synthetic chemistry. The most established TSQ for intracellular
113 imaging, acyl-cyclooctatetraene, and its optimal two-carbon linker to the cyanine fluorophores,
114 were inherited from previous works[33, 34, 42]. Considering that the valency and position of
115 membrane anchors can influence the performance of PM dyes[26, 27], we strategically planned
116 two anchors at the benzene or naphthalene rings to obtain symmetrical probes.

117 The molecular design of PK Mem dyes is substantiated with practical synthetic chemistry
118 within 7 steps from commercial materials. Take PK Mem 590 as an example (Scheme 1), the
119 substituted naphthylhydrazine **2**, produced from commercial material **1**, was converted into
120 intermediate **3** through Fischer indole synthesis. The key intermediate, fluorophore **5**, was
121 synthesized from **3** through alkylation with iodoethanol followed by condensation with
122 diphenylformamidine. The membrane anchor motif was prepared via alkylation and
123 deprotection reactions on precursor **6**, giving a primary amine, **7**. **7** was grafted onto fluorophore
124 **5** by amide bonds to give intermediate **8**. Subsequently, compound **8** was alkylated with 1,3-
125 propanesultone to yield the amphiphilic intermediate **9**, thereby completing the installations of
126 two membrane anchors. Finally, cyclooctatetraenecarboxylic acid (COT-COOH) was coupled
127 to the fluorophore, giving PK Mem 590. Likewise, PK Mem 555, 650, and their non-COT
128 counterparts, Az-Cy dyes, were prepared through similar routes (Fig. S1 and Supplementary
129 scheme 1-6).

130 With the PK Mem dyes in hand, their absorption and emission spectra in different solvents
131 were recorded (Fig. 1B and Table S1). Resembling MemBright dyes, the fluorescence quantum

yields of PK Mem dyes experience a drastic decrease in PBS and a marked increase in DOPC liposomes (Table S1), indicating that the amphiphilic PK Mem dyes could form micelles in aqueous solutions, leading to strong self-quenching in fluorescence. The aggregates of PK Mem dyes undergo disassembly within lipid membranes (Fig. 1C), giving a fluorogenic response to liposomes and cells. The critical micelles concentrations of PK Mem dyes were determined to be approximately 70 nM (Fig. 1D). Compared to micelles in PBS, the fluorescence quantum yields of PK Mem 555, 590, and 650 in DOPC liposomes increased 24-fold, 41-fold, and 180-fold, respectively, demonstrating high fluorogenicity and the potential for wash-free imaging (Table S1).

To investigate the impact of the triplet-state quencher COT on phototoxicity and photostability, PK Mem dyes and MemGlow dyes, bearing the same fluorophores and anchors but with or without COTs were compared in a head-to-head manner. Az-Cy dyes, featuring different connectivity between chromophores and anchors, were also compared. First, photobleaching curves were obtained from imaging fixed HeLa cells to avoid membrane motion artifacts. The bleaching half-life ($\tau_{1/2}$) of PK Mem dyes were 4.0-fold, 14.3-fold, and 5.6-fold longer than that of MemGlow dyes, and 3.2-fold, 5.4-fold, and 6.7-fold longer than that of Az-Cy3/3.5/5, respectively (Fig. 1E and Table S2). Furthermore, their reactive oxygen species (ROS) generations were measured using the 1,3-diphenylisobenzofuran decay assay[46]. Compared to Az dyes, the singlet oxygen quantum yields of PK Mem dyes decreased by 22-31% after conjugation with COT (Fig. 1F and Table S2). These data suggested that COT conjugation to membrane dyes exhibited alleviated phototoxicity and photobleaching.

Imaging of cancer and primary cells

Having the gentle dyes characterized in vitro, we conducted cell labeling experiments to test the specificity of PK Mem dyes on various cells (Fig. 2A). After stained with PK Mem dyes (20 nM) for 5 min, HeLa cells were imaged under confocal microscopy without washing. PK Mem dyes exhibited distinct and intense localization on cell membranes, and the staining process was remarkably rapid (Fig. 2B). In a comparative co-staining experiment, PK Mem dyes achieved specific and bright membrane localization comparable to that of WGA-iFluor™ 488 within 5 min (Fig. S2). PK Mem probes exhibit minimal internalization within 120 min at 37°C (Fig. S3). In confluent HeLa cells co-stained with PK Mem 650 and WGA- iFluor™ 488, the ratio of PK Mem 650 fluorescence intensity to WGA-488 fluorescence intensity was quantified at plasma membrane, cell-cell contacts, and tunneling nanotubes. At cell-cell contacts, PK Mem 650 exhibits approximately two-fold stronger labeling compared to WGA-488 (Fig. S4). By principle, WGA-488 labels the cell membrane through surface polysaccharides, resulting in variations between individual cells. Yet, WGA staining is more sensitive to accessibility due to its bulkier size, giving weaker signal at contact sites. At tunneling nanotubes, PK Mem 650 exhibited over two-fold higher staining selectivity than WGA-488 (Fig. S4). The impact of the probes on the viability of HeLa cells was assessed via CCK-8 assay. PK Mem dyes did not exhibit significant cytotoxicity at a concentration as high as 1 μM which is far above their staining concentrations (Fig. S5). Finally, compatibility with fixation was tested. HeLa cells were either stained after fixation (Fig. S6A) in 4% formaldehyde in PBS or fixed subsequent to staining (Fig. S6B). In both cases specific PM staining can be achieved.

Next, KB cells were treated with PK Mem dyes (20 nM) for 5 min, resulting in a clean and bright fluorescence staining of the cellular membrane (Fig. S7). The strong fluorescence signal of PK Mem dyes enables 3D imaging and z-stack image reconstruction of live KB cells using laser scanning confocal microscopy (Fig. 2C and Fig. S8). PK Mem 555 exhibited distinct staining of tunneling nanotubes involved in intercellular communication (Fig. 2C and Video S1). We next challenged PK Mem dyes with various primary cells and for multicolor imaging. With the prolonged culture time, mESCs exhibited clonogenic growth with tightly arranged cells and an overall spherical shape. When co-stained with WGA-488, PK Mem dyes still exhibited relatively uniform and highly penetrable staining effects, while WGA-488 demonstrated limited diffusion and staining efficiency in densely packed mESCs (Fig. 2D and Fig. S9). A live rat sperm was labeled with PK Mem 555 (200 nM), SPY505-DNA, and SPY650-tubulin for three-color confocal imaging (Fig. 2E). The cell membrane of the sperm wrapped tightly around the axoneme of the flagellum. The tail of the sperm gradually becomes thinner, possibly due to the disappearance of the fibrous sheath[47]. This staining scheme of sperm can withstand formaldehyde fixation (Fig. S10). Alternatively, post-staining labeling of these three dyes can also achieve specific labeling (Fig. S11).

PK Mem dyes can effectively stain isolated hippocampal neurons at a low concentration of 20 nM (Fig. 2F and Fig. S12). Due to their remarkable photostability and minimal phototoxicity, PM dyes enable ultralong-term monitoring of axon growth of hippocampal neurons on DIV1. By capturing one image every two minutes with 0.3% power of a 561 nm laser line, it was feasible to monitor neurons stained with PK Mem 555 (20 nM) for up to 20.5 hours (Video S2).

Membrane imaging was also a routine practice on fixed and permeabilized samples with multi-color immunofluorescence labeling. To test PK Mem dyes on fixed neurons, PK Mem 555 and Phalloidin-AF488 were applied to formaldehyde-fixed and Triton-permeabilized hippocampal neurons, giving the intricate structure of dendritic spines after fixation (Fig. S13A). In another demonstration, PK Mem 555, and a VGluT1 monoclonal antibody targeting glutamatergic axon terminals[48, 49], were applied to a fixed and permeabilized hippocampal neuron. After further incubation with a secondary antibody for VGluT1 (Goat Anti-Rabbit IgG AF647), synapses that release glutamate can be identified on the plasma membrane (Fig. S13B).

By incubating adult mouse cardiomyocytes with PK Mem 555, Hoechst, PK Mito Deep Red and Lyso-Tracker Green, a four-color image under live cell confocal microscopy was recorded (Fig. 2G). The strong fluorescence signal of PK Mem 555 enables the visualization of the cell membrane of adult mouse cardiomyocytes and their distinct cross-striated structure. Additionally, such four-color images can be recorded with adult mouse cardiomyocytes that were stained after fixation or fixed after staining (Fig. S14) with comparable image quality. For neonatal rat cardiomyocytes, PK Mem dyes could also be paired with Hoechst and Lyso-Tracker Green for multiplexed staining (Fig. S15). Overall, PK Mem dyes are bright and reliable stains for various primary cells, are compatible with fixation protocols, and pair well with other fluorescent markers.

Imaging neurons in brain slices and in vivo

Due to the high brightness and fast diffusion speed of PK Mem dyes, we conducted further evaluations of their capabilities in brain slices and *in vivo* two-photon imaging. PK Mem 555 and Hoechst counterstain were applied to mouse brain slices (Fig. 3A) before the slice was

imaged using a confocal microscope. High-quality images of cortical neurons and hippocampal neurons in mouse brain slices can be recorded (Fig. 3B and Video S3). Furthermore, by zooming in on the hippocampal region of the brain slices, the cell bodies and axons of neurons were clearly visible (Fig. 3B).

We further evaluated the potential of PK Mem dyes for *in vivo* imaging in mice using miniature two-photon microscopy with a single 920 nm fixed-wavelength fs-pulsed laser (Fig. 3C). The optical window provided an opportunity for two-photon imaging of awake mice, and the high signal-to-noise ratio of PK Mem 555 facilitated clear visualization of neuronal cell membranes (Fig. 3D). Moreover, blood vessels can be clearly identified in the superficial region of the mouse brain (Fig. S16). Both the brain slice and *in vivo* two-photon images demonstrated that PK Mem 555 preferentially highlights neurons for general fluorescence imaging.

Ultralong-term dynamic imaging of cell membrane morphology, migration and beating with reduced phototoxicity

Phototoxicity-induced cell membrane blebbing and subsequent cell death are common issues during long-term recordings of live cells. We rigorously tested the phototoxicity of PK Mem dyes with imaging-based assays using head-to-head comparisons. HeLa cells labeled with PK Mem 555 or MemGlow 560 were imaged under time-lapse confocal microscopy with identical parameters. A representative movie demonstrated that HeLa cells labeled with PK Mem 555 began to bubble at frame 50, while those labeled with MemGlow 560 bubbled at frame 20 (Fig. 4A). The average cell bubbling time of PK Mem 555 (n=12) labeled cells was twice as long as that of MemGlow 560 (n=10) (Fig. 4B). Similar trends were recorded with PK Mem 590 and MemGlow 590, as well as PK Mem 650 and MemGlow 640 (Fig. S17). Overall, PK Mem dyes generally bear more than three-fold reduced phototoxicity in practical confocal imaging experiments, enabling long-term monitoring of dynamic morphological changes in cell membranes. Notably, such phototoxicity reduction is more pronounced in the live-cell imaging assay than that in ROS generation assay (Fig. 1F), suggesting a rich yet overlooked photochemistry and photobiology.

Previous research has suggested that phototoxicity has a significant impact on cell migration speed[50]. In comparable video recordings, L929 cells labeled with PK Mem 555 and PK Mito Deep Red exhibited rapid migration, accompanied by the formation of retraction fibers and migrasomes throughout the nearly 6 h imaging duration (total 220 recorded frames). In contrast, cells labeled with MemGlow 560 and PK Mito Deep Red showed a compromised migration speed, accompanied by blebbing, mitochondrial deterioration, cell shrinkage, and death. (Fig. 4C and Video S4). The superior performance of PK Mem 555 labeling in time-lapse imaging, as evidenced by the maintenance of cell viability, highlights its privilege in time-lapse imaging and analysis.

We then switched to the recording of the beating process of cardiomyocytes which is orchestrated around plasma membranes. High-temporal-resolution imaging of neonatal rat cardiomyocytes is particularly challenging due to their increased sensitivity to phototoxicity[44]. Phototoxic damage can disrupt cardiomyocyte contractions (Fig. 4D). We employed wide-field microscopy to monitor the contractions of neonatal rat cardiomyocytes labeled with PK Mem 555 at high temporal resolution and high light intensity. Representative time-lapse videos revealed that neonatal rat cardiomyocytes, when labeled with PK Mem 555, ceased beating at

264 frame 10612 while still retaining fluorescence on the membrane until frame 18001. In contrast,
265 neonatal rat cardiomyocytes labeled with MemGlow 560 stopped beating around frame 2875
266 and completely lost fluorescence by frame 5553 (Fig. 4E and Video S5). These findings
267 highlight the biocompatibility of PK Mem dyes for monitoring the physiological processes of
268 sensitive and fragile primary cells. The live-cell imaging assays in this section establish PK
269 Mem dyes as a gentle tool for investigating the intricate physiological dynamics of delicate
270 primary cells.

271

272 *Super-resolution imaging of migrasomes and dendritic spines with STED microscopy*

273 STED is a promising tool for studying cell membranes[51, 52], particularly for imaging smaller
274 membrane structures such as dendritic spines, retraction fibers, and membranous vesicles. Since
275 STED microscopy typically requires higher light intensity than diffraction-limited approaches,
276 phototoxicity and photobleaching can present a significant technical hurdle[53, 54]. Compared to
277 Cy3, the presence of the naphthalene ring in Cy3.5 results in a more red-shifted emission
278 spectrum without compromising photostability, making Cy3.5 an optically privileged
279 chromophore for STED recording using a 775 nm depletion laser[42]. After conjugation with COT
280 to enhance photostability and reduce phototoxicity, PK Mem 590 emerged as a promising probe
281 for STED imaging of cell membrane structures, especially on live cells. Compared to
282 conventional microscopy, STED imaging of the cell membrane of live L929 cells labeled with
283 PK Mem 590 resulted in a clearly resolved membranous structure (Fig. S18).

284 We further studied migrasomes, the migration-dependent membrane-bound vesicular
285 structures generated along retraction fibers in migrating cells, with diameters ranging from 500
286 nm to 3 μm[55]. By staining the cell membrane with PK Mem 590, the nucleus with Hoechst, the
287 mitochondria with PK Mito Deep Red, and the lysosomes with Lyso-Tracker Green respectively,
288 we obtained a four-color image (Fig. S19). PK Mem 590 effectively stained PM, along with the
289 membranous extracellular vesicles such as migrasomes. Upon further magnification, the
290 presence of an intriguing phenomenon of mitocytosis was uncovered, which is a migrasomes-
291 mediated mitochondrial quality control process (Fig. S19)[56]. Following the proposed model
292 where migrasomes are released along with the cell movements, migrasomes of myocardial
293 fibroblasts can be imaged at the retracting end of the cell path. Using PK Mem 590 for STED
294 imaging, migrasomes can be imaged at a sub-100 nm resolution, revealing their presence at the
295 rear or crossroads of cell retraction fibers (Fig. 5A).

296 Moreover, we showcase the capability of PK Mem dyes to track endocytic vesicles. L1-
297 CAM is a marker protein of endocytic vesicles that are related with neurite outgrowth,
298 fasciculation, and migration[57, 58]. PK Mem 555 and L1-CAM monoclonal antibody were applied
299 to live hippocampal neurons, followed by a fluorescent secondary antibody of L1-CAM.
300 Imaging of live antibody uptake and internalization showcased that PK Mem 555 can track
301 endocytic vesicles containing L1-CAM and monitor their internalization, highlighting its
302 capability for monitoring endocytosis through internalization (Fig. S21).

303 Dendritic spines show activity-dependent and developmental regulation of their
304 morphology. By employing STED microscopy, we could visualize axons and dendrites in
305 primary hippocampal neurons labeled with PK Mem 590, particularly with fine details of
306 dendritic spines (Fig. 5C). The implementation of STED microscopy yielded a remarkable
307 enhancement in image resolution, surpassing approximately two-fold increase and providing a

308   more detailed view of their morphology (Fig. 5D-E).

309

310   *Live-cell time-lapse super-resolution imaging of the growth cone and mitochondrial axonal*
311   *transport*

312   During neuronal development, neurons undergo polarization and swiftly extend their axons
313   to form functional neural circuits. As highly dynamic structures located at the axon's tip, growth
314   cones direct axonal pathfinding toward their targets and facilitate axon elongation[59, 60].
315   Practically, PK Mem 590 enables time-lapse STED recordings of growth cones for ~13 frames,
316   which facilitated our understanding of the dynamic structural changes of the growth cone
317   during neuronal migration processes (Fig. 6A and Video S6). Overall, the optical properties of
318   PK Mem 590 render it a recommended probe for super-resolution imaging of PM using STED
319   microscopy.

320   Axonal transport plays a vital role in maintaining neuronal health, in which mitochondria
321   are important cargos. Anterograde transport ensures the transportation of healthy mitochondria
322   from the soma to the axon terminals, while retrograde transport primarily facilitates the transfer
323   of damaged mitochondria back to the soma for degradation and recycling[61, 62]. Structured
324   illumination microscopy (SIM) is suitable for long-term, super-resolution imaging of live cells
325   as it offers higher temporal resolution yet lower phototoxicity compared to STED microscopy[63-
326   66]. During the time-lapse SIM imaging of neurons labeled with PK Mem 555 and PK Mito Deep
327   Red, the mitochondrial bidirectional transports within neuronal axons were monitored for over
328   4 hours (7600 frames) (Fig. 6B, and Video S7). During the long-distance continuous transport
329   of mitochondria, there were frequent occurrences of stationary/dynamic pauses and changes in
330   direction. The elaborately tailored photophysical properties of PK Mem dyes, synergizing the
331   enhanced resolution of SIM imaging, have allowed us to accurately distinguish the fluorescent
332   signals of individual mitochondria within axons.

333

334   **Discussion**

335   On the photophysical chemistry side of the fluorophores, conjugating with COT has been
336   suggested to be a general strategy to reduce the phototoxicity and photobleaching of cyanine
337   dyes. However, the effect of COT on photostability and phototoxicity seems to be largely
338   influenced by the microenvironment. The *in vitro* singlet oxygen generation assay indicated
339   that there was only approximately one-third reduction in the singlet oxygen quantum yields of
340   PK Mem dyes compared with their non-COT counterparts (Table S2 & Fig. S3). However, PK
341   Mem dyes showed more than a three-times decrease in phototoxicity in the live cell experiments
342   of HeLa, L929 and cardiomyocyte (Fig. 4). The discrepancy between *in vitro* and cellular
343   results may be due to differences in the microenvironment surrounding the dye. During the
344   measurement of singlet oxygen quantum yield, the dye is present in a polar protic solvent,
345   whereas in cellular experiments, the dye is surrounded by hydrophobic phospholipid molecules.
346   We speculate that the excited-state energies of the dyes in different microenvironments are not
347   the same. Moreover, in previous studies, the photostability of Cy3-COT conjugates appeared
348   to be similar with the Cy3 counterpart without COT[34, 39]. However, COT conjugated to the
349   membrane-localized Cy3 (as in PK Mem 555) enhanced the photostability by 42% (Table S2).
350   These data collectively suggested that the photochemistry of excited-states is sensitive to the
351   microenvironment, which should be further studied using both rigorous in vitro assays and

352 validated on biological systems.

353 From a cell biology perspective, PK Mem dyes offer bright, specific, fluorogenic, yet gentle
354 imaging of cell membranes. One limitation of PK Mem dyes is that, as amphiphilic organic
355 molecules which have affinities to albumins, the compatibility of PK Mem with FBS is still
356 limited. Adding FBS generally causes a loss of specific fluorescence on the cell membrane. For
357 neurons whose maintenance does not depend on FBS, this issue would be less of a concern.
358 Rather, the low concentration and minimal phototoxicity of PK Mem dyes allow for more
359 physiological monitoring of neuronal activities. In this sense, PK Mem dyes and WGA-dye
360 conjugates supplement and supplant each other as ideal PM stains for different applications.

361 In conclusion, we demonstrate PK Mem dyes as a robust toolkit for general imaging of
362 plasma membranes. These dyes are compatible with various cancer cells or primary cells,
363 enabling live-cell and fixed-cell imaging. Particularly, their reduced phototoxicity and high
364 photostability make them ideal for long-term monitoring of physiological activities on the cell
365 membrane, such as cell migration and cardiomyocyte contraction. PK Mem dyes offer bright
366 neuronal membrane staining at concentrations as low as 20 nM and enable super-resolution
367 imaging of dendritic spines morphology and long-term super-resolution imaging of growth
368 cones extension and mitochondrial transport in axons. We anticipate that PK Mem dyes will
369 become common reagents for membrane imaging in the time-lapse super-resolution era.

370

382

Author Contributions

384 J.L., and Y.L. performed all experiments and data analyses. Z.C. conceived and supervised the
385 project. J.L., Y.L. and Z.C. wrote the paper with input from all authors. Y.F. and P.X. provided
386 experiential guidance for SIM imaging experiments. S.L. provided guidance for the culture of
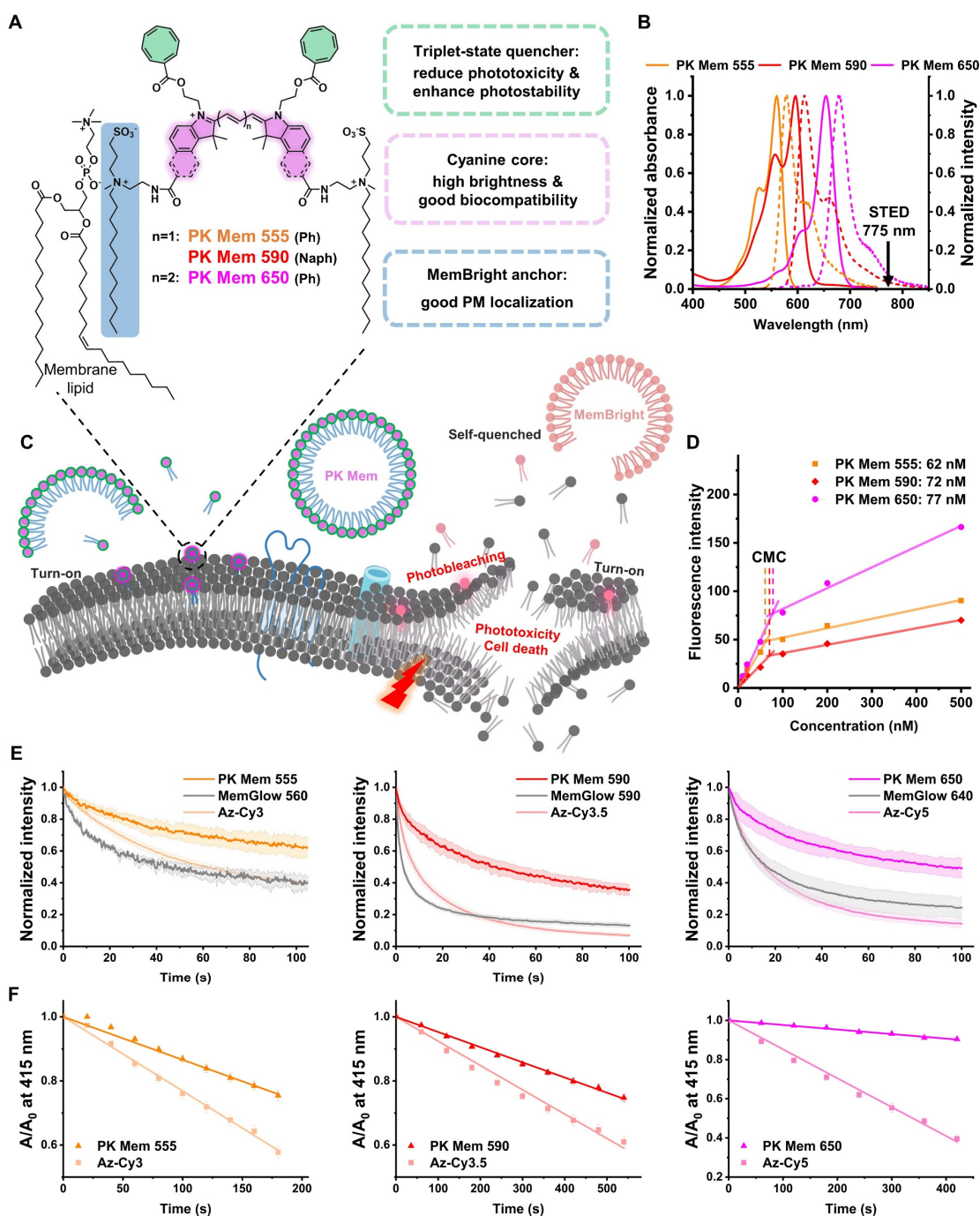387 neurons. L.D. provided mouse sperms. L.H. provided mouse embryonic stem cells.

388

Competing Financial Interests

390 Z.C., Y.L. and J.L. are inventors of a patent application protecting the compounds presented in
391 this study which was submitted by Peking University. Z.C. owns shares of Genvivo tech. The
392 remaining authors declare no competing interests.

393

Figures

Figure 1. PK Mem dyes employ cyclooctatetraenes as triplet-state quenchers to optically strengthen and photodynamically tame the MemBright dyes.

(A) Chemical structures of PK Mem dyes featuring the modular integration of cyclooctatetraenes and amphiphilic anchors to the cyanine palette.

(B) Absorption (solid lines) and emission (dashed lines) spectra of PK Mem dyes in MeOH.

(C) Schemes for the mechanisms of turn-on, photostability, and phototoxicity of PK Mem dyes.

(D) Plot of the maximum fluorescence intensity against the concentration of PK Mem dyes showing their critical micelle concentration (CMC).

404   (E) Photostability comparison among PK Mem dyes, MemGlow, and AZ-Cy labelled on fixed

405   HeLa cells.

406   (F) In vitro detection of reactive oxygen species (ROS) through 1,3-diphenylisobenzofuran

407   decay assay.
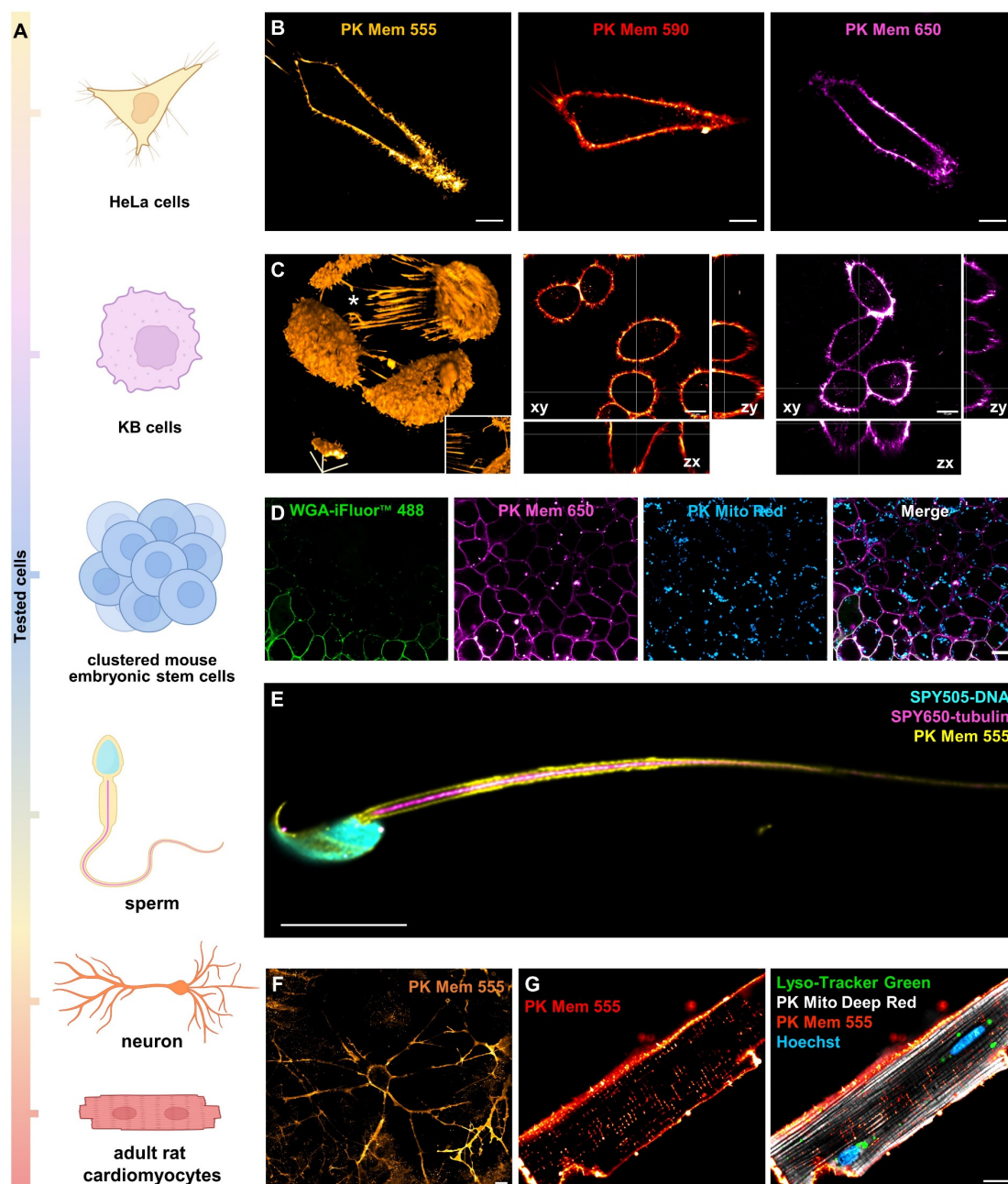
408
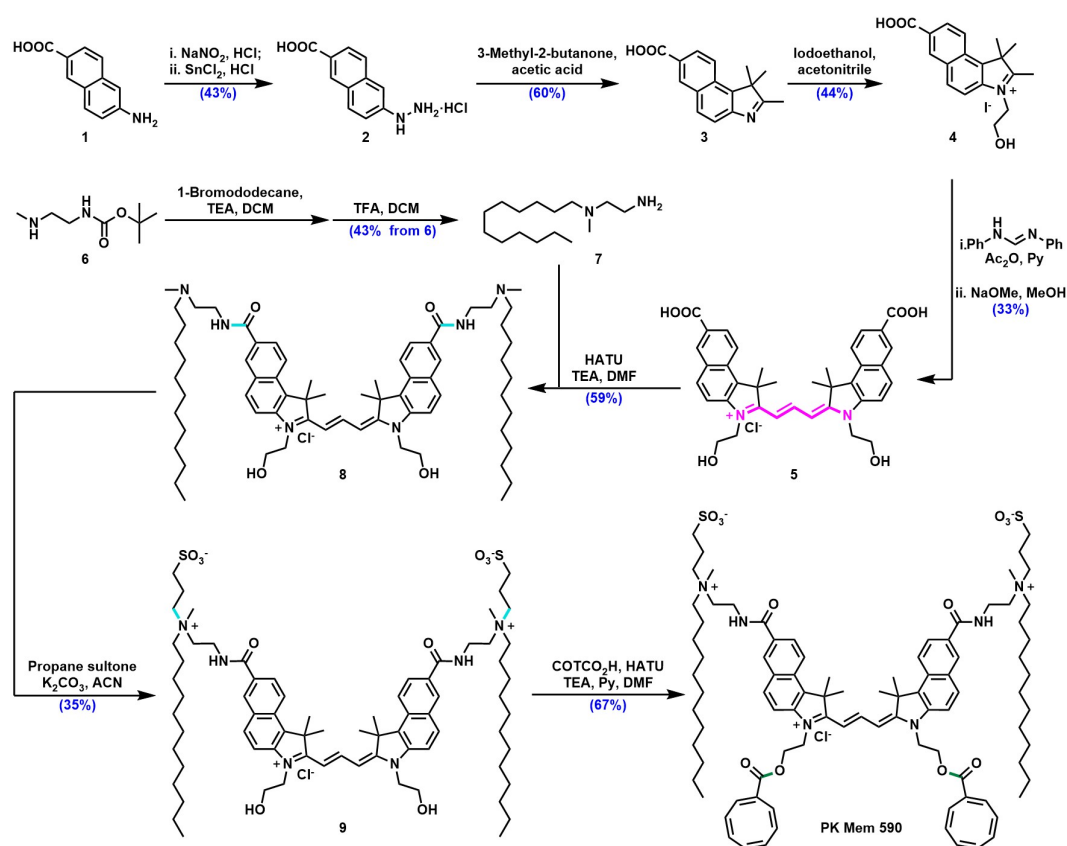
Scheme 1. Synthetic route of PK Mem 590 via a modular derivatization of cyanine dyes with amphiphilic linkers and cyclooctatetraenes.

Figure 2. 2D and 3D confocal imaging of various cells using PK Mem dyes

(A) Cancer and primary cells imaged in this study.

(B) Laser scanning confocal microscopy (LSCM) images of live HeLa cells treated with PK Mem dyes (20 nM) for 5 min without washing. Scale bar = 10 μm.

(C) Left, 3D reconstruction of live KB cells stained with PK Mem dyes. Inset in the left panel is the top view of intercellular nanotubes indicated by an asterisk. Right, orthogonal projection obtained from z stacks. Scale bar = 10 μm.

(D) Multicolor images of live mouse embryonic stem cells (mESC) stained with WGA-488 and PK Mem 650. Mitochondrial was stained with PK Mito Red. Scale bar = 10 μm.

(E) Multicolor image of a live rat sperm labeled with PK Mem 555 (200 nM), SPY505-DNA, and SPY650-tubulin. Scale bar = 10 μm.

13

425   (F) LSCM of live hippocampal primary neurons stained with PK Mem 555 (20 nM, 10 min)

426   without washing. Scale bar = 10 μm.

427   (G) Multicolor image of a live adult rat cardiomyocyte labeled with PK Mem 555 (1 μM),

428   Hoechst, PK Mito Deep Red, and Lyso-Tracker Green. Scale bar = 10 μm.

429

430
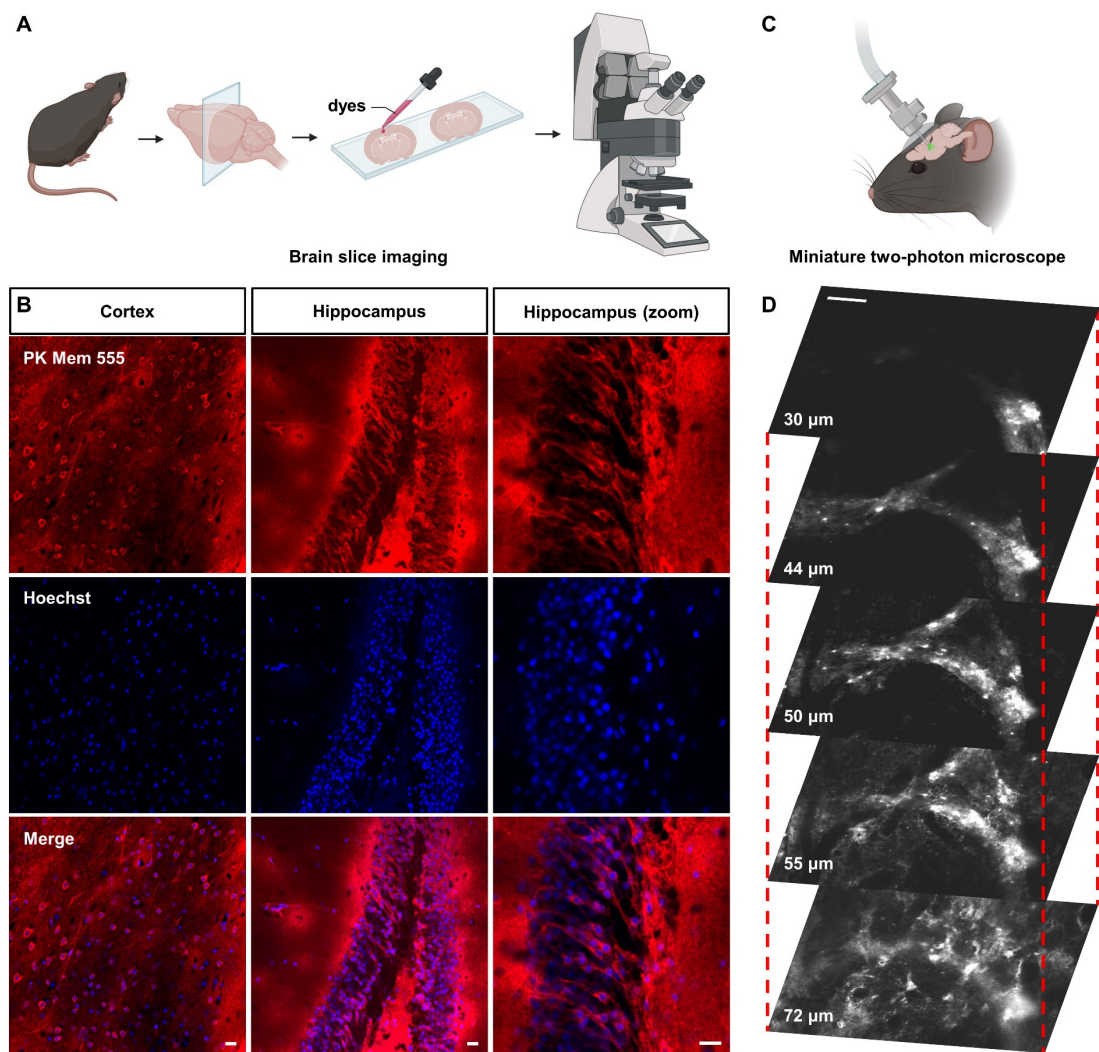
Figure 3. PK Mem 555 stains brain slices and a live mouse brain.

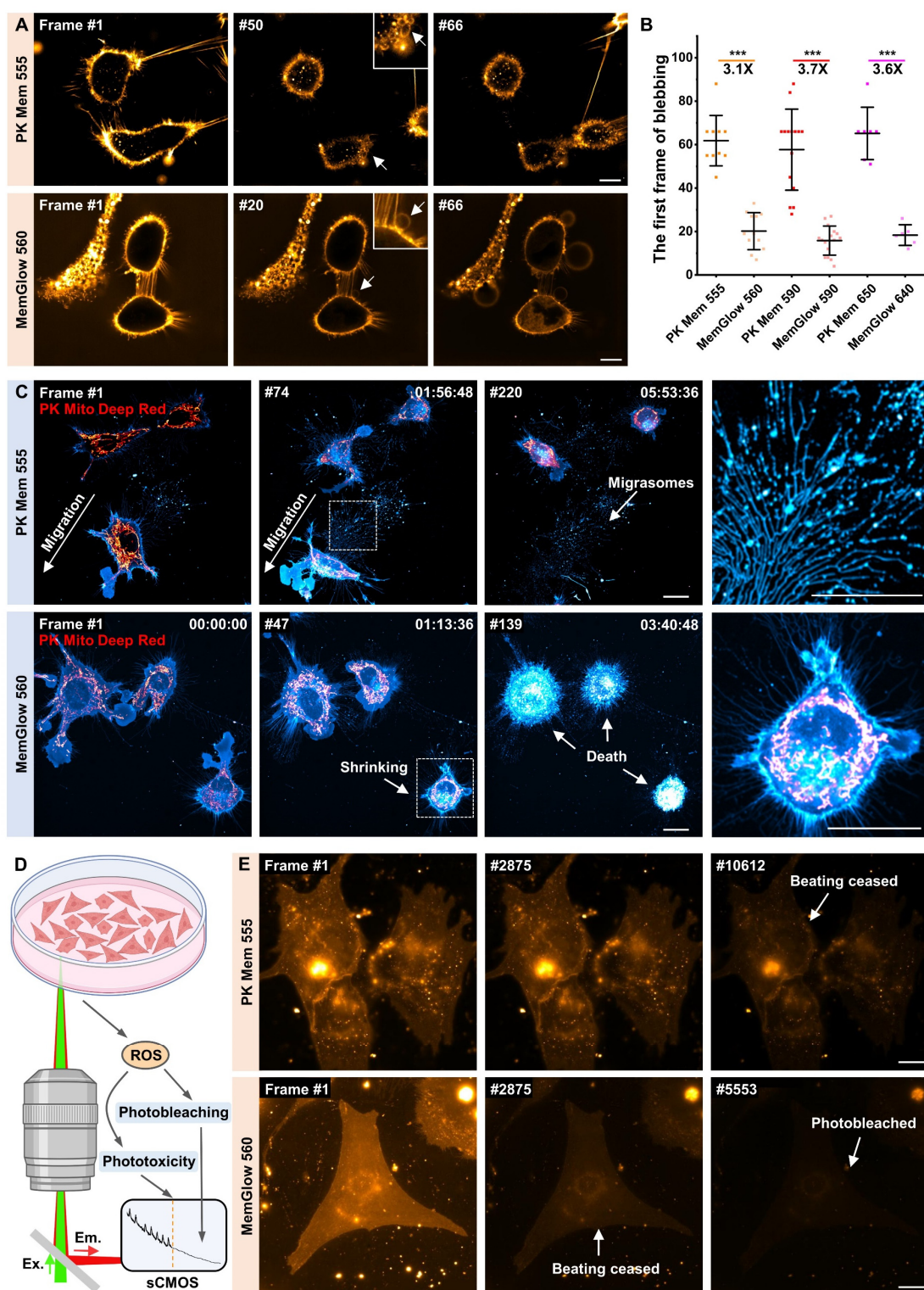(A) Scheme of neuronal imaging of mouse brain slices stained with dyes.

(B) Confocal images of brain slices labeled with PK Mem 555 and Hoechst. Scale bar = 20 μm.

(C) Scheme of the intravital two-photon imaging setup.

(D)Two-photon images of PK Mem 555-labeled neurons in a mouse brain, see also Video. S3.

Scale bar = 50 μm.

439

Figure 4. The low phototoxicity of PK Mem 555 enables long-term recording of cell migration and beating.

(A) Long-term confocal recordings of HeLa cells labeled with MemGlow 560 and PK Mem 555. Blebbing events are highlighted with arrows, indicating photodamage. Scale bar = 10 μm.

16

445   (B) Dot plots of the mean frame number in which the blebs emerge (N>5). Statistical

446   significances were calculated with one-tailed Welch's t-test (or two-tailed for symmetric

447   stimulation), and p values were given for each comparison.

448   (C) Long-term LSCM recordings of L929 cells labeled with MemGlow 560 and PK Mem

449   555. Mitochondria were stained with PK Mito Deep Red. The rightmost images show

450   magnified views of the dashed white boxes in the second column, illustrating migrasomes and

451   shrunken cells. Scale bar = 20 μm.

452   (D) Schematic representation of long-term wide-field recordings of beating neonatal rat

453   cardiomyocytes. Photobleaching diminishes fluorescence signal while phototoxicity can be

454   characterized by the cease of beating.

455   (E) Long-term wide-field recordings of neonatal rat cardiomyocytes labeled with MemGlow

456   560 and PK Mem 555. Scale bar = 10 μm.

457
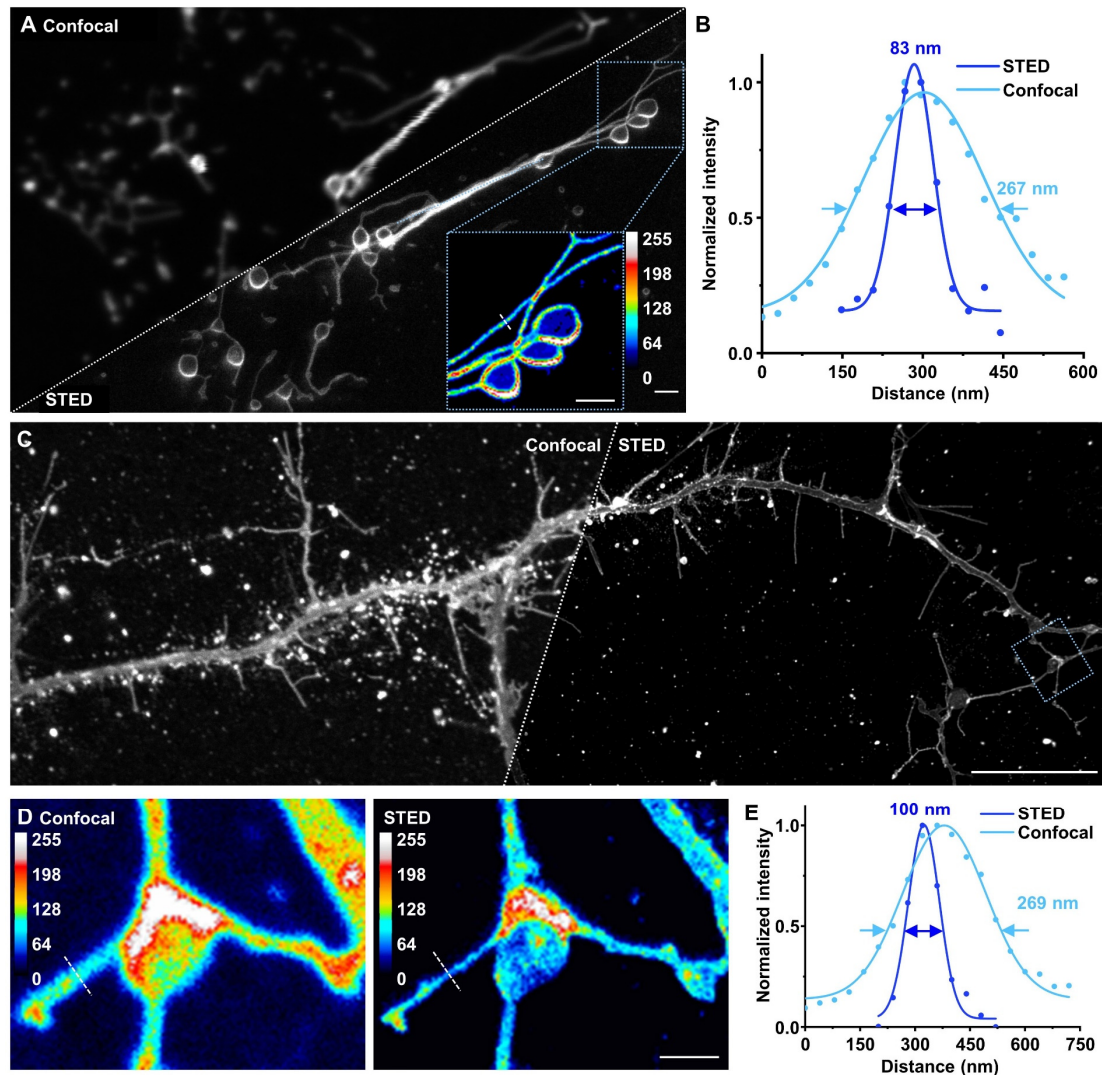
Figure 5. PK Mem 590 enables STED imaging on migrasomes and dendritic spines.

(A) Confocal and STED images of migrasomes from live myocardial fibroblast. Scale bar = 1 μm.
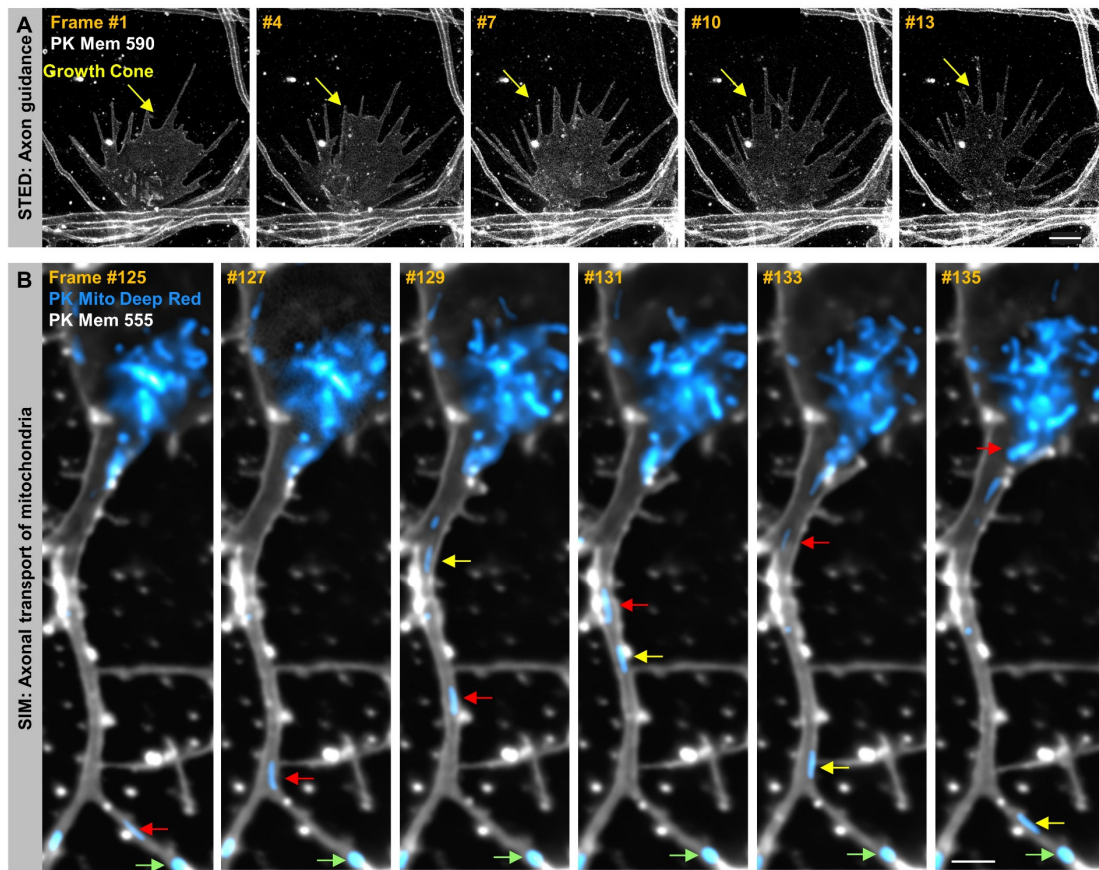
(B) Intensity profiles corresponding to the white dotted line of the STED and confocal images.

(C) Confocal and STED images of axons and dendritic spines from a live hippocampal neuron. Scale bar = 10 μm.

(D) Magnified view of the blue boxed area from Figure C. Scale bar = 1 μm.

(E) Intensity profiles corresponding to the white dotted line of the STED and confocal images.

18

Figure 6. PK Mem dyes enable time-lapse super-resolution imaging of the growth cone and mitochondrial axonal transport.

(A) Time-lapse STED images of the growth cone from the live hippocampal neuron stained with PK Mem 590. The arrow indicates the dynamics of the growth cone. Scale bar = 2 μm.

(B) Time-lapse SIM images (0.5 Hz) of the axon from the live hippocampal neuron stained with PK Mem 555. Mitochondria were stained with PK Mito Deep Red. Anterograde transport (yellow arrow), retrograde transport (red arrow), and stationary/dynamic pause (green arrow) of mitochondria within the axon were indicated. Scale bar = 2 μm.

References

1. Singer, S. J.; Nicolson, G. L., The fluid mosaic model of the structure of cell membranes. *Science* **1972,** *175* (4023), 720-731.

2. Brown, D. A.; Rose, J. K., Sorting of GPI-anchored proteins to glycolipid-enriched membrane subdomains during transport to the apical cell surface. *Cell* **1992,** *68* (3), 533-544.

3. Grecco, Hernán E.; Schmick, M.; Bastiaens, Philippe I. H., Signaling from the living plasma membrane. *Cell* **2011,** *144* (6), 897-909.

4. Groves, J. T.; Kuriyan, J., Molecular mechanisms in signal transduction at the membrane. *Nature Structural & Molecular Biology* **2010,** *17* (6), 659-665.

5. Lemmon, M. A., Membrane recognition by phospholipid-binding domains. *Nature Reviews Molecular Cell Biology* **2008,** *9* (2), 99-111.

6. Collot, M.; Pfister, S.; Klymchenko, A. S., Advanced functional fluorescent probes for cell plasma membranes. *Current Opinion in Chemical Biology* **2022,** *69*, 102161.

7. Fernández-Suárez, M.; Ting, A. Y., Fluorescent probes for super-resolution imaging in living cells. *Nature Reviews Molecular Cell Biology* **2008,** *9* (12), 929-943.

8. Klymchenko, A. S., Fluorescent probes for lipid membranes: from the cell surface to organelles. *Accounts of Chemical Research* **2023,** *56* (1), 1-12.

9. Peters, B. P.; Ebisu, S.; Goldstein, I. J.; Flashner, M., Interaction of wheat germ agglutinin with sialic acid. *Biochemistry* **1979,** *18* (24), 5505-5511.

10. Monsigny, M.; Roche, A.-C.; Sene, C.; Maget-Dana, R.; Delmotte, F., Sugar-lectin interactions: how does wheat-germ agglutinin bind sialoglycoconjugates? *European Journal of Biochemistry* **1980,** *104* (1), 147-153.

11. Chen, L.; Ma, L.; Yu, L., WGA is a probe for migrasomes. *Cell Discovery* **2019,** *5* (1), 13.

12. Collot, M.; Ashokkumar, P.; Anton, H.; Boutant, E.; Faklaris, O.; Galli, T.; Mély, Y.; Danglot, L.; Klymchenko, A. S., Membright: a family of fluorescent membrane probes for advanced cellular imaging and neuroscience. *Cell Chemical Biology* **2019,** *26* (4), 600-614.e7.

13. Shynkar, V. V.; Klymchenko, A. S.; Kunzelmann, C.; Duportail, G.; Muller, C. D.; Demchenko, A. P.; Freyssinet, J.-M.; Mely, Y., Fluorescent biomembrane probe for ratiometric detection of apoptosis. *Journal of the American Chemical Society* **2007,** *129* (7), 2187-2193.

14. Schäfer, B.; Orbán, E.; Borics, A.; Huszár, K.; Nyeste, A.; Welker, E.; Tömböly, C., Preparation of semisynthetic lipoproteins with fluorescent cholesterol anchor and their introduction to the cell membrane with minimal disruption of the membrane. *Bioconjugate Chemistry* **2013,** *24* (10), 1684-1697.

15. Wu, M.-Y.; Leung, J.-K.; Kam, C.; Situ, B.; Wu, Z.-J.; Chou, T. Y.; Feng, S.; Chen, S., Cancer cell-selective aggregation-induced emission probe for long-term plasma membrane imaging. *Cell Reports Physical Science* **2022,** *3* (2), 100735.

16. Hymel, D.; Cai, S.; Sun, Q.; Henkhaus, R. S.; Perera, C.; Peterson, B. R., Fluorescent mimics of cholesterol that rapidly bind surfaces of living mammalian cells. *Chemical Communications* **2015,** *51* (78), 14624-14627.

17. Paloncýová, M.; Aniander, G.; Larsson, E.; Knippenberg, S., Cyanine dyes with tail length asymmetry enhance photoselection: a multiscale study on DiD probes in a liquid disordered membrane. *Spectrochimica Acta Part A: Molecular and Biomolecular Spectroscopy* **2020,** *224*.

18. Klymchenko, Andrey S.; Kreder, R., Fluorescent probes for lipid rafts: from model membranes to living cells. *Chemistry & Biology* **2014,** *21* (1), 97-113.

20

19. Gan, W.-B.; Grutzendler, J.; Wong, W. T.; Wong, R. O. L.; Lichtman, J. W., Multicolor "DiOlistic" labeling of the nervous system using lipophilic dye combinations. *Neuron* **2000,** *27* (2), 219-225.

20. Bolte, S.; Talbot, C.; Boutte, Y.; Catrice, O.; Read, N. D.; Satiat-Jeunemaitre, B., FM-dyes as experimental probes for dissecting vesicle trafficking in living plant cells. *Journal of Microscopy* **2004,** *214* (2), 159-173.

21. Betz, W. J.; Mao, F.; Smith, C. B., Imaging exocytosis and endocytosis. *Current Opinion in Neurobiology* **1996,** *6* (3), 365-371.

22. Zal, T.; Anna Zal, M.; Lotz, C.; Goergen, C. J.; Gascoigne, N. R. J., Spectral shift of fluorescent dye FM4-64 reveals distinct microenvironment of nuclear envelope in living cells. *Traffic* **2006,** *7* (12), 1607-1613.

23. Ferri, G.; Fiume, G.; Pozzi, D.; Caracciolo, G.; Cardarelli, F., Probing the role of nuclear-envelope invaginations in the nuclear-entry route of lipofected DNA by multi-channel 3D confocal microscopy. *Colloids and Surfaces B: Biointerfaces* **2021,** *205*, 111881.

24. Darwich, Z.; Klymchenko, A. S.; Dujardin, D.; Mély, Y., Imaging lipid order changes in endosome membranes of live cells by using a Nile Red-based membrane probe. *RSC Advances* **2014,** *4* (17), 8481-8488.

25. Carravilla, P.; Dasgupta, A.; Zhurgenbayeva, G.; Danylchuk, D. I.; Klymchenko, A. S.; Sezgin, E.; Eggeling, C., Long-term STED imaging of membrane packing and dynamics by exchangeable polarity-sensitive dyes. *Biophysical Reports* **2021,** *1* (2).

26. Collot, M.; Kreder, R.; Tatarets, A. L.; Patsenker, L. D.; Mely, Y.; Klymchenko, A. S., Bright fluorogenic squaraines with tuned cell entry for selective imaging of plasma membrane vs. endoplasmic reticulum. *Chemical Communications* **2015,** *51* (96), 17136-17139.

27. Collot, M.; Boutant, E.; Lehmann, M.; Klymchenko, A. S., BODIPY with tuned amphiphilicity as a fluorogenic plasma membrane probe. *Bioconjugate Chemistry* **2019,** *30* (1), 192-199.

28. Laissue, P. P.; Alghamdi, R. A.; Tomancak, P.; Reynaud, E. G.; Shroff, H., Assessing phototoxicity in live fluorescence imaging. *Nature Methods* **2017,** *14* (7), 657-661.

29. Wäldchen, S.; Lehmann, J.; Klein, T.; van de Linde, S.; Sauer, M., Light-induced cell damage in live-cell super-resolution microscopy. *Scientific Reports* **2015,** *5* (1), 15348.

30. Stephens, D. J.; Allan, V. J., Light microscopy techniques for live cell imaging. *Science* **2003,** *300* (5616), 82-86.

31. Song, L.; Varma, C. A.; Verhoeven, J. W.; Tanke, H. J., Influence of the triplet excited state on the photobleaching kinetics of fluorescein in microscopy. *Biophysical Journal* **1996,** *70* (6), 2959-2968.

32. Zheng, Q.; Jockusch, S.; Zhou, Z.; Blanchard, S. C., The contribution of reactive oxygen species to the photobleaching of organic fluorophores. *Photochemistry and Photobiology* **2014,** *90* (2), 448-454.

33. Zheng, Q.; Jockusch, S.; Zhou, Z.; Altman, R. B.; Zhao, H.; Asher, W.; Holsey, M.; Mathiasen, S.; Geggier, P.; Javitch, J. A.; Blanchard, S. C., Electronic tuning of self-healing fluorophores for live-cell and single-molecule imaging. *Chemical Science* **2017,** *8* (1), 755-762.

34. Yang, Z.; Li, L.; Ling, J.; Liu, T.; Huang, X.; Ying, Y.; Zhao, Y.; Zhao, Y.; Lei, K.; Chen, L.; Chen, Z., Cyclooctatetraene-conjugated cyanine mitochondrial probes minimize phototoxicity in fluorescence and nanoscopic imaging. *Chemical Science* **2020,** *11* (32), 8506-8516.

35. Liu, F.; Danylchuk, D. I.; Andreiuk, B.; Klymchenko, A. S., Dynamic covalent chemistry in live cells for organelle targeting and enhanced photodynamic action. *Chem Sci* **2022,** *13* (13), 3652-3660.

36. Bulina, M. E.; Chudakov, D. M.; Britanova, O. V.; Yanushevich, Y. G.; Staroverov, D. B.;

Chepurnykh, T. V.; Merzlyak, E. M.; Shkrob, M. A.; Lukyanov, S.; Lukyanov, K. A., A genetically encoded photosensitizer. *Nature Biotechnology* **2006,** *24* (1), 95-99.

37. Hoebe, R. A.; Van Oven, C. H.; Gadella, T. W. J.; Dhonukshe, P. B.; Van Noorden, C. J. F.; Manders, E. M. M., Controlled light-exposure microscopy reduces photobleaching and phototoxicity in fluorescence live-cell imaging. *Nature Biotechnology* **2007,** *25* (2), 249-253.

38. Zhang, Y.; Ling, J.; Liu, T.; Chen, Z., Lumos maxima – how robust fluorophores resist photobleaching? *Current Opinion in Chemical Biology* **2024,** *79*, 102439.

39. Altman, R. B.; Terry, D. S.; Zhou, Z.; Zheng, Q.; Geggier, P.; Kolster, R. A.; Zhao, Y.; Javitch, J. A.; Warren, J. D.; Blanchard, S. C., Cyanine fluorophore derivatives with enhanced photostability. *Nature Methods* **2012,** *9* (1), 68-71.

40. Grimm, J. B.; English, B. P.; Chen, J.; Slaughter, J. P.; Zhang, Z.; Revyakin, A.; Patel, R.; Macklin, J. J.; Normanno, D.; Singer, R. H.; Lionnet, T.; Lavis, L. D., A general method to improve fluorophores for live-cell and single-molecule microscopy. *Nature Methods* **2015,** *12* (3), 244-250.

41. Zhang, Y.; Yang, C.; Peng, S.; Ling, J.; Chen, P.; Ma, Y.; Wang, W.; Chen, Z.; Chen, C., General strategy to improve the photon budget of thiol-conjugated cyanine dyes. *Journal of the American Chemical Society* **2023,** *145* (7), 4187-4198.

42. Liu, T.; Stephan, T.; Chen, P.; Keller-Findeisen, J.; Chen, J.; Riedel, D.; Yang, Z.; Jakobs, S.; Chen, Z., Multi-color live-cell STED nanoscopy of mitochondria with a gentle inner membrane stain. *Proceedings of the National Academy of Sciences* **2022,** *119* (52), e2215799119.

43. Grenier, V.; Martinez, K. N.; Benlian, B. R.; García-Almedina, D. M.; Raliski, B. K.; Boggess, S. C.; Maza, J. C.; Yang, S. J.; Gest, A. M. M.; Miller, E. W., Molecular Prosthetics for Long-Term functional imaging with fluorescent reporters. *ACS Central Science* **2022,** *8* (1), 118-121.

44. Liu, S.; Ling, J.; Chen, P.; Cao, C.; Peng, L.; Zhang, Y.; Ji, G.; Guo, Y.; Chen, P. R.; Zou, P.; Chen, Z., Orange/far-red hybrid voltage indicators with reduced phototoxicity enable reliable long-term imaging in neurons and cardiomyocytes. *Proceedings of the National Academy of Sciences* **2023,** *120* (34), e2306950120.

45. Liu, T.; Kompa, J.; Ling, J.; Lardon, N.; Zhang, Y.; Chen, J.; Reymond, L.; Chen, P.; Tran, M.; Yang, Z.; Zhang, H.; Liu, Y.; Pitsch, S.; Zou, P.; Wang, L.; Johnsson, K.; Chen, Z., Gentle rhodamines for live-cell fluorescence microscopy. *bioRxiv* **2024**, 2024.02.06.579089.

46. Entradas, T.; Waldron, S.; Volk, M., The detection sensitivity of commonly used singlet oxygen probes in aqueous environments. *Journal of Photochemistry and Photobiology B: Biology* **2020,** *204*, 111787.

47. Leung, M. R.; Zeng, J.; Wang, X.; Roelofs, M. C.; Huang, W.; Zenezini Chiozzi, R.; Hevler, J. F.; Heck, A. J. R.; Dutcher, S. K.; Brown, A.; Zhang, R.; Zeev-Ben-Mordehai, T., Structural specializations of the sperm tail. *Cell* **2023,** *186* (13), 2880-2896.e17.

48. Kaneko, T.; Fujiyama, F., Complementary distribution of vesicular glutamate transporters in the central nervous system. *Neuroscience Research* **2002,** *42* (4), 243-50.

49. Fremeau, R. T.; Troyer, M. D.; Pahner, I.; Nygaard, G. O.; Tran, C. H.; Reimer, R. J.; Bellocchio, E. E.; Fortin, D.; Storm-Mathisen, J.; Edwards, R. H., The expression of vesicular glutamate transporters defines two classes of excitatory synapse. *Neuron* **2001,** *31* (2), 247-260.

50. Kiepas, A.; Voorand, E.; Mubaid, F.; Siegel, P. M.; Brown, C. M., Optimizing live-cell fluorescence imaging conditions to minimize phototoxicity. *Journal of Cell Science* **2020,** *133* (4).

51. Carravilla, P.; Dasgupta, A.; Zhurgenbayeva, G.; Danylchuk, D. I.; Klymchenko, A. S.;

Sezgin, E.; Eggeling, C., Long-term STED imaging of membrane packing and dynamics by exchangeable polarity-sensitive dyes. *Biophysical Reports* **2021,** *1* (2), 100023.

52. Eggeling, C.; Willig, K. I.; Barrantes, F. J., STED microscopy of living cells – new frontiers in membrane and neurobiology. *Journal of Neurochemistry* **2013,** *126* (2), 203-212.

53. Kilian, N.; Goryaynov, A.; Lessard, M. D.; Hooker, G.; Toomre, D.; Rothman, J. E.; Bewersdorf, J., Assessing photodamage in live-cell STED microscopy. *Nature Methods* **2018,** *15* (10), 755-756.

54. Sigal, Y. M.; Zhou, R.; Zhuang, X., Visualizing and discovering cellular structures with super-resolution microscopy. *Science* **2018,** *361* (6405), 880-887.

55. Ma, L.; Li, Y.; Peng, J.; Wu, D.; Zhao, X.; Cui, Y.; Chen, L.; Yan, X.; Du, Y.; Yu, L., Discovery of the migrasome, an organelle mediating release of cytoplasmic contents during cell migration. *Cell Research* **2015,** *25* (1), 24-38.

56. Jiao, H.; Jiang, D.; Hu, X.; Du, W.; Ji, L.; Yang, Y.; Li, X.; Sho, T.; Wang, X.; Li, Y.; Wu, Y. T.; Wei, Y. H.; Hu, X.; Yu, L., Mitocytosis, a migrasome-mediated mitochondrial quality-control process. *Cell* **2021,** *184* (11), 2896-2910.e13.

57. Dequidt, C.; Danglot, L.; Alberts, P.; Galli, T.; Choquet, D.; Thoumine, O., Fast turnover of L1 adhesions in neuronal growth cones involving both surface diffusion and exo/endocytosis of L1 molecules. *Molecular Biology of the Cell* **2007,** *18* (8), 3131-43.

58. Kamiguchi, H.; Lemmon, V., Neural cell adhesion molecule L1: signaling pathways and growth cone motility. *Journal of Neuroscience Research* **1997,** *49* (1), 1-8.

59. Lowery, L. A.; Vactor, D. V., The trip of the tip: understanding the growth cone machinery. *Nature Reviews Molecular Cell Biology* **2009,** *10* (5), 332-343.

60. Stoeckli, E. T., Understanding axon guidance: are we nearly there yet? *Development* **2018,** *145* (10).

61. Sheng, Z.-H.; Cai, Q., Mitochondrial transport in neurons: impact on synaptic homeostasis and neurodegeneration. *Nature Reviews Neuroscience* **2012,** *13* (2), 77-93.

62. Saxton, W. M.; Hollenbeck, P. J., The axonal transport of mitochondria. *Journal of Cell Science* **2012,** *125* (9), 2095-2104.

63. Gustafsson; Agard; Sedat, I5M: 3D widefield light microscopy with better than 100 nm axial resolution. *Journal of Microscopy* **1999,** *195* (1), 10-16.

64. Li, D.; Shao, L.; Chen, B.-C.; Zhang, X.; Zhang, M.; Moses, B.; Milkie, D. E.; Beach, J. R.; Hammer, J. A.; Pasham, M.; Kirchhausen, T.; Baird, M. A.; Davidson, M. W.; Xu, P.; Betzig, E., Extended-resolution structured illumination imaging of endocytic and cytoskeletal dynamics. *Science* **2015,** *349* (6251), aab3500.

65. Huang, X.; Fan, J.; Li, L.; Liu, H.; Wu, R.; Wu, Y.; Wei, L.; Mao, H.; Lal, A.; Xi, P.; Tang, L.; Zhang, Y.; Liu, Y.; Tan, S.; Chen, L., Fast, long-term, super-resolution imaging with Hessian structured illumination microscopy. *Nature Biotechnology* **2018,** *36* (5), 451-459.

66. Cao, R.; Li, Y.; Chen, X.; Ge, X.; Li, M.; Guan, M.; Hou, Y.; Fu, Y.; Xu, X.; Leterrier, C.; Jiang, S.; Gao, B.; Xi, P., Open-3DSIM: an open-source three-dimensional structured illumination microscopy reconstruction platform. *Nature Methods* **2023,** *20* (8), 1183-1186.